Microwave quantum illumination with a digital phase-conjugated receiver

1st Shabir Barzanjeh
Institute for Quantum Science and Technology
Department of Physics and Astronomy
University of Calgary
2500 University Dr. NW, Calgary, AB T2N 1N4, Canada
shabir.barzanjeh@ucalgary.ca

2nd Stefano Pirandola
Department of Computer Science
University of York
York YO10 5GH, UK
stefano.pirandola@york.ac.uk

3rd David Vitali
Physics Division, School of Science and Technology
University of Camerino
Camerino (MC), Italy
david.vitali@unicam.it

4th Johannes Fink
Institute of Science and Technology Austria
3400 Klosterneuburg, Austria
johannes.fink@ist.ac.at

***Abstract*—Quantum illumination is a sensing technique that employs entangled signal-idler beams to improve the detection efficiency of low-reflectivity objects in environments with large thermal noise. The advantage over classical strategies is evident at low signal brightness, a feature which could make the protocol an ideal prototype for non-invasive scanning or low-power short-range radar. Here we experimentally investigate the concept of quantum illumination at microwave frequencies, by generating entangled fields using a Josephson parametric converter which are then amplified to illuminate a room-temperature object at a distance of 1 meter. Starting from experimental data, we simulate the case of perfect idler photon number detection, which results in a quantum advantage compared to the relative classical benchmark. Our results highlight the opportunities and challenges on the way towards a first room-temperature application of microwave quantum circuits.**

***Index Terms*—microwave detection, radar, quantum signals, entanglement**

I. Introduction

Many applications of quantum sensing are naturally embedded in the microwave regime. A prominent example is quantum illumination (QI) [1]–[9] for its remarkable robustness to background noise, which at room temperature amounts to $\sim 10^3$ thermal quanta per mode at a few GHz. The aim of QI is to detect a low-reflectivity object in the presence of very bright thermal noise. This is accomplished by probing the target with less than one entangled photon per mode, in a non-invasive fashion which is impossible to reproduce with classical means. In the Gaussian QI protocol [2], the light is prepared in a two mode squeezed vacuum state [10] with the signal mode sent to probe the target while the idler mode is kept at the receiver. Even though entanglement is lost in the round trip from the target, the surviving signal-idler correlations, when appropriately measured, can be strong enough to beat the performance achievable by the most powerful classical detection strategy. In the low brightness regime, where QI shows the biggest advantage, it could be suitable for extending quantum sensing techniques to short-range radar [11] and non-invasive diagnostic scanner applications [12].

Previous experiments relied directly on the measurement of field quadratures, and in the microwave domain Refs. [13] and [14] demonstrated a quantum enhancement of the detected covariances compared to a symmetric classical noise radar, i.e. with approximately equal signal and idler photon number. When the phase of the reflected signal is stable over relevant timescales or it is a priori known, homodyne detection of field quadratures, where the signal is mixed with a local oscillator with the same frequency and with a stable and tunable phase, represents the optimal field detection and the strongest classical benchmark. Due to this appropriate phase-sensitive detection, an ideal classically correlated noise radar can be on par or, in the case of a bright idler [8], even outperform coherent heterodyne detection, which is the optimal choice maximizing the signal-to-noise (SNR) in the case of uncontrollable, phase-rotating targets. In this latter case the two field quadratures are measured simultaneously, with the unavoidable addition of 3 dB of quantum noise.

In this work, we implement a digital version of the phase-conjugated receiver of Ref. [15], experimentally investigating

This work was supported by the Institute of Science and Technology Austria (IST Austria), the European Research Council under grant agreement number 758053 (ERC StG QUNNECT) and the EU's Horizon 2020 research and innovation programme under grant agreement number 862644 (FET Open QUARTET). S.B. acknowledges support from the Marie Skłodowska Curie fellowship number 707438 (MSC-IF SUPEREOM), DV acknowledge support from EU's Horizon 2020 research and innovation programme under grant agreement number 732894 (FET Proactive HOT) and the Project QuaSeRT funded by the QuantERA ERANET Cofund in Quantum Technologies, and J.M.F from the Austrian Science Fund (FWF) through BeyondC (F71), a NOMIS foundation research grant, and the EU's Horizon 2020 research and innovation programme under grant agreement number 732894 (FET Proactive HOT).

Conference paper based on Ref. [9], Sh. Barzanjeh *et al., Microwave quantum illumination using a digital receiver*.

978-1-7281-8942-0/20/$31.00 2020 IEEE

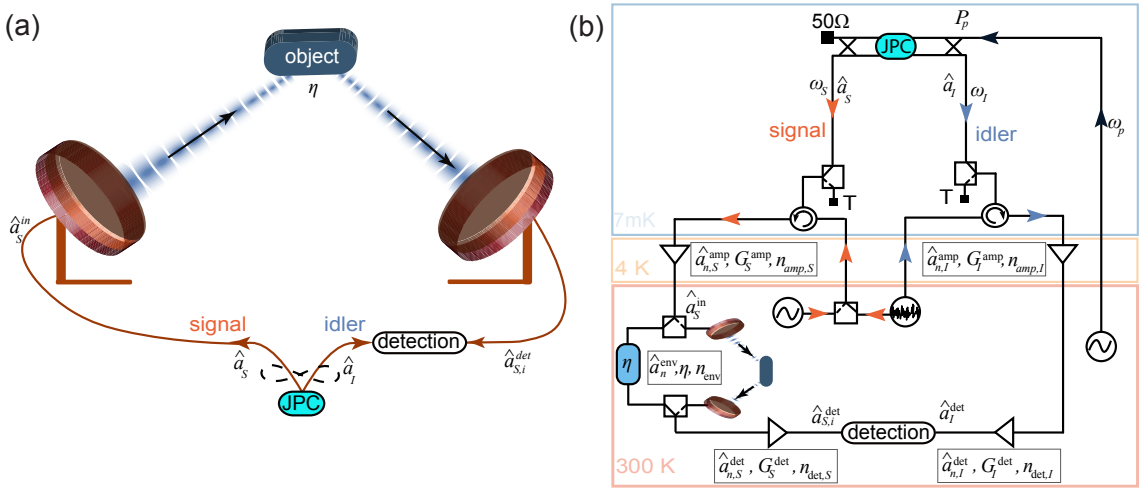

Fig. 1. **Implementation of microwave quantum illumination.** (a) A quantum source generates and emits stationary entangled microwave fields in two separate paths. The signal mode $\hat{a}_S$ is used to interrogate the presence ($i = 1$) or absence ($i = 0$) of a room-temperature object with total round-trip reflectivity η. The returned mode $\hat{a}_{S,i}^{\mathrm{det}}$ is measured together with the unperturbed idler mode $\hat{a}_I$. (b) Circuit diagram of the experimental setup. A superconducting Josephson parametric converter (JPC) is used to entangle signal and idler modes at frequencies ω_S and ω_I by applying a suitable parametric pump tone at the sum frequency $\omega_p = \omega_S + \omega_I$ at ~ 7 mK. A coherent microwave tone or a classically correlated noise source are used to generate benchmark signals at room temperature that are sent into the dilution refrigerator and reflected from the JPC ports. The outputs of the JPC or the reflected classical signals are amplified, down-converted and digitized simultaneously and independently for both channels. The signal mode passes through a measurement line that contains a room-temperature switch that is used to select between a digitally controllable attenuator η and a free-space link realized with two antennas and a movable reflective object.

proof of concept QI in the microwave regime [16]. We use a Josephson parametric converter (JPC) [17], [18] inside a dilution refrigerator at 7 mK for entanglement generation [19], [20]. The generated signal microwave mode, with annihilation operator $\hat{a}_S$, is amplified by a HEMT amplifier at 4 K to facilitate its detection, and sent to probe a target placed in the noisy environment at room-temperature, while the idler mode $\hat{a}_I$ is measured as shown in Fig. 1. The reflection from the target $\hat{a}_R$ is also detected, and the two measurement results are post-processed to calculate the SNR for discriminating the presence or absence of the object. Our experimental implementation of QI relies on linear quadrature measurements and suitable post-processing in order to compute all covariance matrix elements from the full measurement record as shown in previous microwave quantum optics experiments with linear detectors [21]–[23]. This enables the digital simulation of the phase-conjugated receiver of Ref. [15], exploiting the correlations of the JPC output fields without the explicit use of analog photodetection. We then compare the resulting SNR with the SNR of other detection strategies employing the same signal path and the same signal photon numbers at the JPC output. This means comparing our detection strategy not with the ultimate classical benchmark, but with the best classical benchmark operating under the same conditions and amplification/measurement chain.

Our digital approach to QI circumvents common practical problems such as finite idler storage time that can limit the range and fidelity of QI detection schemes. However, this advantage comes at the expense that the theoretically strongest classical benchmark in the same conditions - the coherent state homodyne detector using the same signal power and signal path - can be approached in specific conditions such as quantum limited amplification, but never be outperformed. To outperform coherent state homodyne detection in practice, will require low temperature square law detection of microwave fields that can be realized with radiometer or photon counting measurements, even though in this latter case idler storage is again needed. Nevertheless, using calibration measurements of the idler path, we can simulate a situation with perfect idler photon number detection, extrapolating the case where the reflected mode is detected together with the idler mode using analog microwave photon counters. For this situation we show that the SNR of coherent heterodyne detection and symmetric noise radars is exceeded by up to 4 dB and that of homodyne detection - the classical benchmark - by up to 1 dB for the same amplified signal path, measurement bandwidth and signal power. We also note that the strong and noisy amplification of the signal path chosen to facilitate the detection with commercial analog-to-digital converters enables another classical receiver strategy, i.e. the detection of the amplifier noise in the presence of the target. Since the amplified noise exceeds the environmental noise at room temperature by orders of magnitude, this would indeed be the most effective strategy for the implemented experiment. For the same reason, a low noise coherent source at room temperature would outperform the relative benchmarks considered here. In practice, outperforming the room temperature benchmark depends on the chosen amount of gain, the type of amplifier and the loss in the detection system and therefore does not pose a fundamental limitation to the presented measurement scheme that focusses on the relative comparison of the different illumination types.

II. Results

The experimental setup, shown in Fig. 1(b), is based on a frequency tunable superconducting JPC operated in the three-wave mixing regime and pumped at the sum of signal and idler frequencies $\omega_p = \omega_S + \omega_I$. The output of the JPC contains a nonzero phase-sensitive cross correlation $\langle \hat{a}_S \hat{a}_I \rangle$, which is a signature of the entanglement between the signal mode with frequency $\omega_S = 10.09$ GHz and the idler mode with frequency $\omega_I = 6.8$ GHz. The quantities $\langle \hat{O} \rangle$ and $(\Delta O_i)^2 = \langle \hat{O}_i^2 \rangle - \langle \hat{O}_i \rangle^2$ define the mean and the variance of the operator $\hat{O}$, respectively, and they are evaluated from experimental data. The signal and idler are sent through two different measurement lines, where they are amplified, filtered, down-converted to an intermediate frequency of 20 MHz and digitized with a sampling rate of 100 MHz using an 8 bit analog-to-digital converter. Applying fast Fourier transform and post-processing to the measured data, we obtain the quadrature voltages I_i and Q_i, which are related to the complex amplitudes a_i and their conjugate a_i^* of the signal and idler modes at the outputs of the JPC as $a_i = \frac{I_i + \mathrm{i}\, Q_i}{\sqrt{2\hbar\omega_i B R G_i}}$ and $a_i^* = \frac{I_i - \mathrm{i}\, Q_i}{\sqrt{2\hbar\omega_i B R G_i}}$, having the same measurement statistics as the annihilation operator $\hat{a}_i$. Here, $R = 50\,\Omega$, $B = 200$ kHz is the measurement bandwidth set by a digital filter and $i = S, I$ [23]–[25]. We have calibrated the system gain and noise of both measurement channel, obtaining $(G_S, G_I) = (93.98(01), 94.25(02))$ dB and $(n_{\mathrm{add},S}, n_{\mathrm{add},I}) = (9.61(04), 14.91(1))$ respectively.

A first important check for the experiment is to quantify the amount of entanglement at the output of the JPC at 7 mK. A sufficient condition for the signal and idler modes to be entangled is the non-separability criterion [26] $\Delta := \langle \hat{X}_-^2 \rangle + \langle \hat{P}_+^2 \rangle < 1$, for the joint field quadratures $\hat{X}_- = (\hat{a}_S + \hat{a}_S^\dagger - \hat{a}_I - \hat{a}_I^\dagger)/2$ and $\hat{P}_+ = (\hat{a}_S - \hat{a}_S^\dagger + \hat{a}_I - \hat{a}_I^\dagger)/(2\mathrm{i})$. In Fig. 2(a) we show measurements of Δ as a function of the signal photon number $N_S = \langle \hat{a}_S^\dagger \hat{a}_S \rangle$ at the output of the JPC at millikelvin temperatures, as obtained by applying the above calibration procedure to both signal and idler modes, and compare the result with classically-correlated radiation. The latter is generated at room temperature using the white noise mode of an arbitrary waveform generator, divided into two different lines, individually up-converted to the signal ω_S and idler ω_I frequencies and fed to the JPC inside the dilution refrigerator. Note that, for both JPC and classically correlated noise, we digitally rotate the relative phase of the quadratures to maximize the correlation between signal and idler.

The classically-correlated signal and idler modes are then reflected back from the JPC (pumps are off) and pass through the measurement lines attached to the outputs of the JPC. This ensures that both classical and quantum radiations experience the same conditions in terms of gain, loss, and noise before reaching the target and before being detected in the identical way. As shown in Fig. 2(a), at low photon number the parameter Δ is below one proving that the outputs of the JPC are entangled, while at larger photon number (larger pump power) the entanglement gradually degrades and vanishes at $N_S = 4.5$ photons $\cdot \mathrm{s}^{-1} \cdot \mathrm{Hz}^{-1}$. We attribute this to finite losses in the JPC, which leads to pump power dependent heating and results in larger variances of the output field. The classically correlated radiation of the same signal power on the other hand (red data points), cannot fulfill the non-separability criterion and therefore $\Delta \geq 1$ for the entire range of the signal photons.

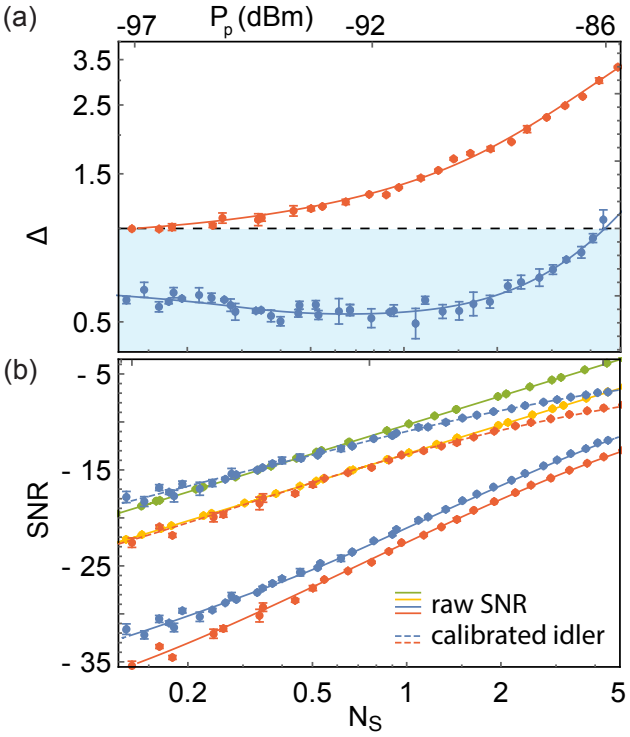

Fig. 2. **Entanglement and quantum illumination.** (a) The measured entanglement parameter Δ for the output of the JPC (blue) and classically-correlated noise (red) as a function of the inferred signal photon number N_S at the output of the JPC and the pump power P_p at the input of the JPC. (b) Comparison of the measured single mode signal-to-noise ratio (SNR) of quantum illumination (QI, solid blue), symmetric classically-correlated illumination (CI, solid red), coherent-state illumination with homodyne (solid green) and heterodyne detection (solid yellow), and the inferred SNR of calibrated QI (dashed blue) and CI (dashed red) as a function of the signal photon number N_S for a perfectly reflective object and a 5 μs measurement time. The dots are measured and inferred data points and the solid and dashed lines are the theory prediction. For both panels (a) and (b) the error bars indicate the 95% confidence interval based on 3 sets of measurements, each with 380 k two channel quadrature pairs for QI/CI, and 192 k quadrature pairs for coherent-state illumination.

The experiments of QI and classically-correlated illumination (CI) are implemented in a similar way, see Fig. 1(b). The two amplified quadratures of the idler mode $\hat{a}_I^{\mathrm{det}}$ are measured at room temperature, and the signal mode $\hat{a}_S$ is amplified (with gain G_S^{amp} and the noise mode $\hat{a}_{n,S}^{\mathrm{amp}}$) and used to probe a noisy region that is suspected to contain an object. In this process, we define η as the total detection loss on the signal path between the two room-temperature switches used in the measurement chain, which includes cable loss, free-space loss, and object reflectivity. The reflected signal from the region is measured, by means of a mixer and an amplifier with gain G_S^{det} and the noise mode $\hat{a}_{n,S}^{\mathrm{det}}$. The output $\hat{a}_{S,i}^{\mathrm{det}}$ in the presence ($i = 1$) or absence ($i = 0$) of the object is then post-processed for the

reconstruction of the covariance matrix of the detected signal-idler state.

The signal mode $\hat{a}_{S,i}^{\rm det}$ takes different forms depending on the presence

$$\hat{a}_{S,1}^{\rm det} = \sqrt{G_S}\left(\sqrt{\eta}\hat{a}_S + \sqrt{\frac{\eta(G_S^{\rm amp}-1)}{G_S^{\rm amp}}}\hat{a}_{n,S}^{\rm amp\dagger} + \sqrt{\frac{1-\eta}{G_S^{\rm amp}}}\hat{a}_n^{\rm env} + \sqrt{\frac{G_S^{\rm det}-1}{G_S}}\hat{a}_{n,S}^{\rm det\dagger}\right), \quad (1)$$

or absence

$$\hat{a}_{S,0}^{\rm det} = \sqrt{G_S^{\rm det}}\Big(\hat{a}_n^{\rm env} + \sqrt{1-\frac{1}{G_S^{\rm det}}}\hat{a}_{n,S}^{\rm det\dagger}\Big), \quad (2)$$

of the target with $\hat{a}_n^{\rm env}$ is the environmental noise mode. In the absence of the object, the signal contains only noise $n_0 = G_S^{\rm det} n_{\rm env} + (G_S^{\rm det}-1)n_{{\rm det},S}$ in which $n_{{\rm det},S}$ is the amplifier added noise after interrogating the object region. In the presence of the target and for $\eta \ll 1$, the added noise to the signal is $n_1 = \eta\, G_S^{\rm det}(G_S^{\rm amp}-1)n_{{\rm amp},S} + n_0$, whose first term is due to the amplifier added noise of the first amplification stage before reaching the target, which exceeds the environmental noise $n_{\rm env}$ as well as the signal photon numbers used to probe the target. This implies that in our proof of principle demonstration the optimal classical strategy would actually be based on detecting the presence or absence of the amplifier noise rather than the coherences and correlations of the signal-idler path with the measured ${\rm SNR}_{\rm passive} = (n_1-n_0)/(n_0+1) \simeq 31.4\,{\rm dB}$ for the chosen gain and receiver noise in our setup. However, for lower noise temperature signal amplifiers and lower gain as well as in longer range applications with increased loss, such a passive signature of the detection scheme will be drastically reduced and eventually disappear in the environmental noise at room temperature.

The final step of the measurement is the application of a digital version of the phase-conjugate receiver [15]. The reflected mode $\hat{a}_{S,i}^{\rm det}$ is first phase-conjugated, and then combined with the idler mode on a 50-50 beam splitter. The SNR of the balanced difference photodetection measurement reads

$${\rm SNR}_{\rm QI/CI} = \frac{(\langle\hat{N}_1\rangle - \langle\hat{N}_0\rangle)^2}{2\left(\sqrt{(\Delta N_1)^2}+\sqrt{(\Delta N_0)^2}\right)^2}, \quad (3)$$

where $\hat{N}_i = \hat{a}_{i,+}^\dagger\hat{a}_{i,+} - \hat{a}_{i,-}^\dagger\hat{a}_{i,-}$ with $\hat{a}_{i,\pm} = (\hat{a}_{S,i}^{\rm det\dagger} + \sqrt{2}\hat{a}_v \pm \hat{a}_I^{\rm det})/\sqrt{2}$ is the annihilation operator of the mixed signal and idler modes at the output of the beam splitter in the absence ($i=0$) and the presence ($i=1$) of the target (here $\hat{a}_v$ is the vacuum noise operator). For the raw SNR without idler calibration we use Eq. (3). In order to simulate perfect photon number detection of the idler mode directly at the JPC output we reduce the variance in the denominator of Eq. (3) by the calibrated idler vacuum and amplifier noise as $\langle\hat{a}_I^\dagger\hat{a}_I\rangle = \langle\hat{a}_i^{\rm det\dagger}\hat{a}_i^{\rm det}\rangle/G_I - (n_{{\rm add},I}+1)$.

The experiment of coherent state illumination is performed by generating a weak coherent tone using a microwave source at room temperature followed by low temperature chain of thermalized attenuators inside the dilution refrigerator. The center frequency of the coherent tone is ω_S, exactly matched with the frequency of the signal used in the QI and CI experiments. The coherent tone is reflected back from the unpumped JPC and directed into the same measurement chain identical to that of QI and CI, see Fig. 1(b). The signal is sent to probe a target region and the detected radiation $\hat{a}_{S,i}^{\rm det}$ is used to calculate the SNR of the digital homodyne and heterodyne detections for the same probe power, bandwidth and amplifier noise.

In the absence of a passive signature due to signal noise amplification, digital homodyne detection of a coherent state represents the optimal classical strategy in terms of the SNR, which is given by

$${\rm SNR}_{\rm CS}^{\rm hom} = \frac{(\langle\hat{X}_{S,1}^{\rm det}\rangle - \langle\hat{X}_{S,0}^{\rm det}\rangle)^2}{2\Big(\sqrt{(\Delta X_{S,1}^{\rm det})^2}+\sqrt{(\Delta X_{S,0}^{\rm det})^2}\Big)^2}, \quad (4)$$

while the SNR of the digital heterodyne detection is lower and given by

$${\rm SNR}_{\rm CS}^{\rm het} = \frac{(\langle\hat{X}_{S,1}^{\rm det}\rangle - \langle\hat{X}_{S,0}^{\rm det}\rangle)^2 + (\langle\hat{P}_{S,1}^{\rm det}\rangle - \langle\hat{P}_{S,0}^{\rm det}\rangle)^2}{2\Big(\sum_{i=1}^{2}\sqrt{(\Delta X_{S,i}^{\rm det})^2+(\Delta P_{S,i}^{\rm det})^2}\Big)^2}, \quad (5)$$

where $\hat{X}_{S,i}^{\rm det} = \frac{\hat{a}_{S,i}^{\rm det}+\hat{a}_{S,i}^{\rm det\dagger}}{\sqrt{2}}$ and $\hat{P}_{S,i}^{\rm det} = \frac{\hat{a}_{S,i}^{\rm det}-\hat{a}_{S,i}^{\rm det\dagger}}{i\sqrt{2}}$ are the field quadrature operators.

In Fig. 2(b) we compare the SNR of QI and CI with and without idler calibration for a perfectly reflective object in a zero loss channel $\eta = 1$. For comparison, we also include the results of coherent-state illumination with homodyne and heterodyne detection. In all cases the signal mode at room temperature is overwhelmed with amplifier noise. For the same measurement bandwidth and using the raw data of the measured quadrature pairs (solid lines) QI (blue dots) outperforms sub-optimum symmetric CI (red dots) by up to 3 dB at low signal photon numbers but it cannot compete with the SNR obtained with coherent state illumination (yellow and green dots). Under the assumption of perfect idler photon number detection, i.e. applying the calibration discussed above (dashed lines), the SNR of QI is up to 4 dB larger than that of symmetric CI and coherent-state illumination with heterodyne detection, which does not require phase information, over the region where the outputs of the JPC are entangled. For signal photon numbers $N_S > 4.5$, where there is no entanglement present in the signal source, the sensitivity of the coherent-state transmitter with heterodyne detection outperforms QI and CI, confirming the critical role of entanglement to improve the sensitivity of the detection.

QI with a phase conjugate receiver is potentially able to outperform coherent-state illumination with homodyne detection by up to 3 dB, i.e. the optimum classical benchmark, in the regime of low signal photon numbers. In the region $N_S < 0.4$

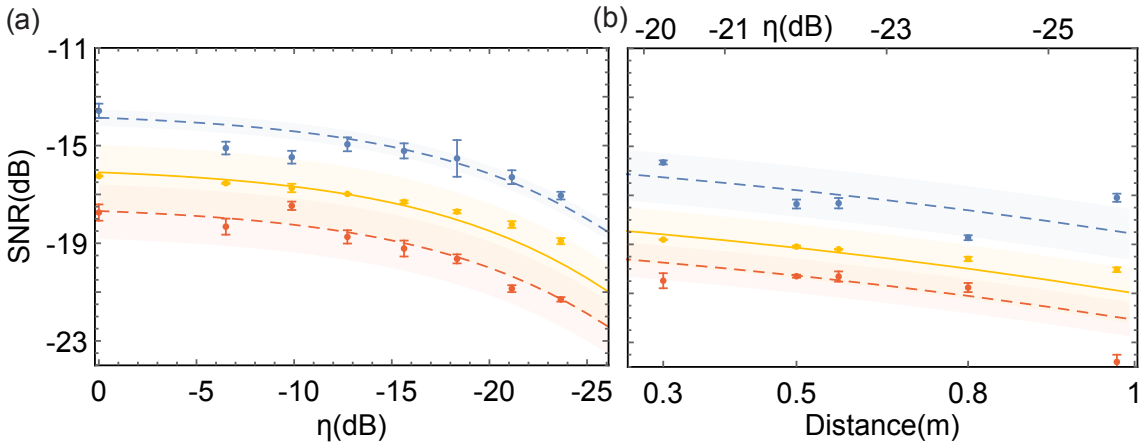

Fig. 3. **Low reflectivity quantum correlated noise radar.** The inferred signal to noise ratio (SNR) of calibrated QI (blue) and symmetric CI (red), and the measured coherent-state illumination with digital heterodyne detection (yellow) as a function of (a) the total signal loss η and (b) object distance from the transmitting and receiving antennas for free space illumination. The error bars are calculated similar to Fig. 2. For both panels the signal photon number is $N_S = 0.5$. The shaded regions are the theoretical uncertainties extracted by fitting the experimental data. The SNR of the coherent state with homodyne detection is not presented in this figure since the expected advantage at the chosen N_S is smaller than systematic errors in this measurement.

the experimentally inferred SNR of QI is approximately 1 dB larger, in agreement with the theoretical prediction taking into account experimental non-idealities like the finite squeezing of the source. In practice though, i.e. without the applied idler calibration, the quantum advantage compared to coherent homodyne detection is not accessible with a digital receiver based on heterodyne measurements, even in the case of quantum limited amplifiers, due to the captured idler vacuum noise, which lowers the optimal SNR by at least 3 dB [2], [6]. The experimental results (dots) are in very good agreement with the theoretical prediction (solid and dashed lines). For the theory we rewrite the SNRs Eqs. (3)-(5) in terms of the signal photon number $N_S = \langle \hat{a}_S^\dagger \hat{a}_S \rangle$, the idler photon number $N_I = \langle \hat{a}_I^\dagger \hat{a}_I \rangle$, and the signal-idler correlation $\langle \hat{a}_S \hat{a}_I \rangle$ at the output of the JPC. These parameters are extracted from the measured and calibrated data as a function of the JPC pump power. Together with the known system gain and noise we plot the theoretical predictions of the various protocols at room-temperature.

An important feature of a radar or short range scanner is its resilience with respect to signal loss. To verify this, as shown in Fig. 1(b), we use two microwave switches at room temperature in the signal line in order to select between a digitally controllable step attenuator to mimic an object with tunable reflectivity and a proof of principle radar setup. With this setup we determine the effects of loss and object reflectivity as well as target distance on the efficiency of the quantum enhanced radar. In Fig. 3(a) we plot the measured SNR of QI, CI and coherent-state illumination with heterodyne detection, as a function of the imposed loss on the signal mode. The calibrated QI protocol is always superior to calibrated symmetric CI and coherent-state illumination with heterodyne detection for a range of effective loss -25 dB $< \eta <$ 0 dB. The dashed lines are the theory predictions from Eq. (3) and Eq. (5) for a fixed chosen signal photon number $N_S = 0.5$. The shaded regions represent the confidence interval extracted from the standard deviation of the measured idler photon numbers and the cross-correlations as a function of η.

In the context of radar, small improvements in the SNR lead to the exponentially improved error probability $\mathcal{E} = 1/2\,\mathrm{erfc}(\sqrt{\mathrm{SNR} \cdot M})$, where $M = T_{\mathrm{tot}} B$ is the number of single mode measurements, and T_{tot} is the total measurement time required for a successful target detection. To test the principle of microwave QI in free-space at room temperature, we amplify and send the microwave signal emitted from JPC to a horn antenna and a copper plate representing the target at a variable distance. The reflected signal from this object is collected using a second antenna of the same type, down-converted, digitized, and combined with the calibrated idler mode to calculate the SNR of the binary decision. With this setup we repeat the measurement for CI and coherent state illumination with heterodyne. Fig. 3(b) shows the SNR of these protocols as a function of the object distance from the transmitting antenna as well as the total loss of the free space link. Calibrated QI reveals higher sensitivity for a reflective target up to 1 meter away from the transmitting antenna. The results are in good agreement with the theoretical model.

Conclusion

In this work we have studied proof of concept quantum illumination in the microwave domain, the most natural frequency range for target detection. Assuming perfect idler photon number detection we showed that a quantum advantage is possible despite the entanglement-breaking signal path. Since the best results are achieved for less than one mean photon per mode, our experiment indicates the potential of QI as non-invasive scanning method, e.g. for biomedical applications, imaging of human tissues or non-destructive rotational spectroscopy of proteins, besides its potential use as short-range low-power radar, e.g. for security applications. However, for this initial proof of principle demonstration the amplified bright noise in

the target region overwhelms the environmental noise by orders of magnitude, which precludes the non-invasive character at short target distances and presents an opportunity to use the presence or absence of the amplifier noise to detect the object with even higher SNR. The use of quantum limited parametric amplifiers [27]–[29] with limited gain, such that the amplified vacuum does not significantly exceed environmental or typical electronic noise at the target, may help to achieve a practical advantage with respect to the lowest noise-figure coherent state heterodyne receivers at room temperature and, up to the vacuum noise, they will also render the idler calibration obsolete. The use of sensitive radiometers or microwave single photon detectors [30]–[32] at millikelvin temperatures without signal amplification, represents a promising route to achieve an advantage in practical situations and with respect to ideal coherent state homodyne receivers. One advantage of the presented digital implementation of QI is that it does not suffer from the idler storage problem of receivers that rely on analog photodetection schemes, inherently limiting the accessible range when used as a radar. It is an interesting open question what other types of receivers [33] could be implemented in the microwave domain, based on state of the art superconducting circuit technology and digital signal processing.

REFERENCES

[1] S. Lloyd, Enhanced sensitivity of photodetection via quantum illumination. *Science* **321**, 1463-1465 (2008).

[2] Si-Hui Tan, Baris I. Erkmen, Vittorio Giovannetti, Saikat Guha, Seth Lloyd, Lorenzo Maccone, Stefano Pirandola, Jeffrey H. Shapiro, Quantum illumination with Gaussian States. *Phys. Rev. Lett.* **101**, 253601 (2008).

[3] E. D. Lopaeva, I. Ruo Berchera, I. P. Degiovanni, S. Olivares, G. Brida, M. Genovese, Experimental Realization of Quantum Illumination. *Phys. Rev. Lett.* **110**, 153603 (2013).

[4] Zheshen Zhang, Maria Tengner, Tian Zhong, Franco N. C. Wong, Jeffrey H. Shapiro, Entanglement's Benefit Survives an Entanglement-Breaking Channel. *Phys. Rev. Lett.* **111**, 010501 (2013).

[5] Zheshen Zhang, Sara Mouradian, Franco N. C. Wong, Jeffrey H. Shapiro, Entanglement-Enhanced Sensing in a Lossy and Noisy Environment. *Phys. Rev. Lett.* **114**, 110506 (2015).

[6] C. Weedbrook, S. Pirandola, J. Thompson, V. Vedral, M. Gu, How discord underlies the noise resilience of quantum illumination. *New Journal of Physics* **18**, 043027 (2016).

[7] S. Pirandola, B. R. Bardhan, T. Gehring, C. Weedbrook, S. Lloyd, Advances in Photonic Quantum Sensing. *Nat. Photon.* **12**, 724-733 (2018).

[8] Jeffrey H. Shapiro, The Quantum Illumination Story. *IEEE Aerospace and Electronic Systems Magazine* **35**, 8-20, (2020).

[9] S. Barzanjeh, S. Pirandola, D. Vitali, J. M. Fink, Microwave quantum illumination using a digital receiver. *Sci. Adv.* **6**, eabb0451 (2020).

[10] C. Weedbrook, S. Pirandola, R. Garcia-Patron, N. J. Cerf, T. C. Ralph, J. H. Shapiro, S. Lloyd, Gaussian quantum information. *Rev. Mod. Phys.* **84**, 621-669 (2012).

[11] J. Choi, V. Va, N. Gonzalez-Prelcic, R. Daniels, C. R. Bhat, R. W. Heath, Millimeter-Wave Vehicular Communication to Support Massive Automotive Sensing. *IEEE Communications Magazine* **54**, 160 (2016). Page(s): 160 - 167

[12] J.C. Lin, Microwave sensing of physiological movement and volume change: A review. *Bioelectromagnetics* **13**, 557 (1992).

[13] C. W. Sandbo Chang, A. M. Vadiraj, J. Bourassa, B. Balaji, C. M. Wilson, Quantum-enhanced noise radar. *Appl. Phys. Lett.* **114**, 112601 (2019).

[14] D. Luong, C. W. Sandbo Chang, A. M. Vadiraj, A. Damini, C. M. Wilson, B. Balaji, Receiver Operating Characteristics for a Prototype Quantum Two-Mode Squeezing Radar. *IEEE Transactions on Aerospace and Electronic Systems* **56**, 2041-2060 (2020).

[15] Saikat Guha, Baris I. Erkmen, Gaussian-state quantum-illumination receivers for target detection. *Phys. Rev. A* **80**, 052310 (2009).

[16] Shabir Barzanjeh, Saikat Guha, Christian Weedbrook, David Vitali, Jeffrey H. Shapiro, Stefano Pirandola, Microwave quantum illumination. *Phys. Rev. Lett.* **114**, 080503 (2015).

[17] N. Bergeal, R. Vijay, V.E. Manucharyan, I. Siddiqi, R. Schoelkopf, S. Girvin, M. Devoret, Phase-preserving amplification near the quantum limit with a Josephson ring modulator. *Nat. Phys.* **6**, 296 (2010).

[18] B. Abdo, A. Kamal, M. H. Devoret, Nondegenerate three-wave mixing with the Josephson ring modulator. *Phys. Rev. B* **87**, 014508 (2013).

[19] E. Flurin, N. Roch, F. Mallet, M. Devoret, B. Huard, Generating entangled microwave radiation over two transmission lines. *Phys. Rev. Lett.* **109**, 183901 (2012).

[20] Matti Silveri, Evan Zalys-Geller, Michael Hatridge, Zaki Leghtas, Michel H. Devoret, S. M. Girvin, Theory of remote entanglement via quantum-limited phase-preserving amplification. *Phys. Rev. A* **93**, 062310 (2016).

[21] Marcus P. da Silva, Deniz Bozyigit, Andreas Wallraff, Alexandre Blais, Schemes for the observation of photon correlation functions in circuit QED with linear detectors. *Phys. Rev. A* **82**, 043804 (2010).

[22] D. Bozyigit, C. Lang, L. Steffen, J. M. Fink, C. Eichler, M. Baur, R. Bianchetti, P. J. Leek, S. Filipp, M. P. da Silva, A. Blais, A. Wallraff, Antibunching of microwave-frequency photons observed in correlation measurements using linear detectors. *Nat. Phys.* **7**, 154 (2011).

[23] C. Eichler, D. Bozyigit, A. Wallraff, Characterizing quantum microwave radiation and its entanglement with superconducting qubits using linear detectors. *Phys. Rev. A* **86**, 032106 (2012).

[24] S. Barzanjeh, E. S. Redchenko, M. Peruzzo, M. Wulf, D. P. Lewis, G. Arnold, J. M. Fink, Stationary entangled radiation from micromechanical motion. *Nature* **570**, 480-483 (2019).

[25] E. P. Menzel, R. Di Candia, F. Deppe, P. Eder, L. Zhong, M. Ihmig, M. Haeberlein, A. Baust, E. Hoffmann, D. Ballester, K. Inomata, T. Yamamoto, Y. Nakamura, E. Solano, A. Marx, R. Gross, Path entanglement of continuous-variable quantum microwaves. *Phys. Rev. Lett.* **109**, 250502 (2012).

[26] L.-M. Duan, G. Giedke, J. I. Cirac, P. Zoller, Inseparability criterion for continuous variable systems. *Phys. Rev. Lett.* **84**, 2722-2725 (2000).

[27] B. Yurke, L. R. Corruccini, P. G. Kaminsky, L. W. Rupp, A. D. Smith, A. H. Silver, R. W. Simon, E. A. Whittaker, Observation of parametric amplification and deamplification in a Josephson parametric amplifier. *Phys. Rev. A* **39**, 2519-2533 (1989).

[28] M. A. Castellanos-Beltran, K. W. Lehnert, Widely tunable parametric amplifier based on a superconducting quantum interference device array resonator. *Appl. Phys. Lett.* **91**, 083509 (2007).

[29] C. Macklin, K. O'Brien, D. Hover, M. E. Schwartz, V. Bolkhovsky, X. Zhang, W. D. Oliver, I. Siddiqi, A near-quantum-limited Josephson traveling-wave parametric amplifier. *Science* **350**, 307 (2015).

[30] S. Kono, K. Koshino, Y. Tabuchi, A. Noguchi, Y. Nakamura, Quantum non-demolition detection of an itinerant microwave photon. *Nat. Phys.* **14**, 546-549, (2018).

[31] Jean-Claude Besse, Simone Gasparinetti, Michele C. Collodo, Theo Walter, Philipp Kurpiers, Marek Pechal, Christopher Eichler, Andreas Wallraff, Single-shot quantum nondemolition detection of individual itinerant microwave photons, *Phys. Rev. X* **8**, 021003 (2018).

[32] Raphael Lescanne, Samuel Deleglise, Emanuele Albertinale, Ulysse Reglade, Thibault Capelle, Edouard Ivanov, Thibaut Jacqmin, Zaki Leghtas, Emmanuel Flurin, Detecting itinerant microwave photons with engineered non-linear dissipation. *Phys. Rev. X* **10**, 021038 (2020).

[33] Quntao Zhuang, Zheshen Zhang, Jeffrey H. Shapiro, Optimum Mixed-State Discrimination for Noisy Entanglement-Enhanced Sensing. *Phys. Rev. Lett.* **118**, 040801 (2017).